Indonesian Physical Review
Volume 07 Issue 03, September 2024
P-ISSN: 2615-1278, E-ISSN: 2614-7904

Morlet's Wavelet analysis on El Niño Southern Oscillation (ENSO) and the Indian Ocean Dipole (IOD) for 84 years: 1940-2023

Suhadi[1*], Jamiatul Khairunnisa Putri[1], Iskhaq Iskandar[2], Supari[3], Muhammad Irfan[2], Melly Ariska[4], Hamdi Akhsan[4]

[1] *Physics Study Program, Universitas Islam Negeri Raden Fatah Palembang, South Sumatra, Indonesia.*
[2] *Department of Physics, Faculty of Mathematics and Natural Sciences, Sriwijaya University, Indonesia.*
[3] *Indonesia Agency for Meteorology, Climatology and Geophysics (BMKG), Indonesia.*
[4] *Physics Education Department, Faculty of Teacher Training and Education Universitas Sriwijaya, Indonesia.*

Corresponding Authors E-mail: suhadi@radenfatah.ac.id

Article Info

Article info:
Received: 12-07-2024
Revised: 22-09-2024
Accepted: 23-09-2024

Keywords:
El Niño Southern Oscillation; Indian Ocean Dipole; Wavelet Analysis; IOD-Like; Indonesia

How To Cite:
Suhadi, J. K. Putri, I. Iskandar, Supari, M. Irfan, M. Ariska, H. Akhsan, "Morlet's Wavelet analysis on El Niño Southern Oscillation (ENSO) and the Indian Ocean Dipole (IOD) for 84 years: 1940-2023", Indonesian Physical Review, vol. 7, no. 3, p 552-561, 2024.

DOI:
https://doi.org/10.29303/ipr.v7i3.363.

Abstract

As is known, the impact caused by El Niño Southern Oscillation (ENSO) and the Indian Ocean Dipole (IOD) can reach extreme levels, especially rainfall in Indonesia. So, updating information on events and cycles of these phenomena is essential. Using Sea Surface Temperature (SST) data spanning the previous 84 years (1940–2023) from ERA5, we examined Sea Surface Temperature Anomalies (SSTA), which serve as a predictive tool for ENSO and IOD events. Apart from that, in this research, SSTA variance analysis was also carried out using Wavelet. The analysis results show several Positive IOD-Like events (1943, 1944, 1977, 1996) and Negative IOD-Like (1985, 1992, 2016). Apart from that, the results of this research also show that El Niño in 2002/03 coincided with Negative IOD in 2002. The results of Wavelet analysis show that the SSTA DMI variance experienced increased activity in the periods 1940-1968, 1969-1991, and 1992-2023. The Wavelet analysis also shows that ENSO activity increased in 1970-2000 and decreased again in 2000-2023.

Copyright (c) 2024 by Author(s), This work is licensed under a Creative Commons Attribution-ShareAlike 4.0 International License.

Introduction

Globally, some phenomena control the climate, i.e. El Niño Southern Oscillation (ENSO) and the Indian Ocean Dipole (IOD). ENSO and IOD are Sea Surface Temperature Anomaly (SSTA) that occur in the Pacific Ocean and the Indian Ocean, respectively. The SSTA is an inherent occurrence caused by the interaction between the ocean and the atmosphere. The Pacific

Walker circulation is, in actuality, a key element of the world climate system. It links the climate variability from the other ocean basins to the mid-and high-latitudes with the variability of the Pacific SST [1-5]. The term Pacific Walker's Circulation or PWC (Indian Walker's Circulation or IWC) is used to refer to Walker's Circulation in the Pacific (Indian) ocean. Differential air pressure in the western or eastern regions initiates the process of PWC formation. Increasing the strength of the Easterly Wind leads to greater movement of Walker's Circulation, which subsequently causes the SST in the Western (Eastern) Pacific Rim to diverge from its normal temperature by becoming warmer (colder). The warmer (colder) SST in a sea region e.g., Indonesian's sea, triggers the gain (weaken) convection water mass activity. Consequently, this leads to an abundance of rainfall in the Indonesian area [2]. In contrast, the Westerly Wind has caused a decline in Walker's circulation, leading to below-average SST in the western (eastern) part of the Pacific Rim [2]. This circumstance has resulted in a scarcity of precipitation inside the borders of Indonesia. An SSTA refers to a deviation from the normal temperature, either colder or warmer. A positive (negative) SSTA is thereafter referred to as El Niño (La Niña). El Niño and La Niña are commonly referred to as ENSO. Typically, ENSO intensifies during the summer (June-August) and reaches its highest point in December through spring (March-May) [6]. Periodically, ENSO occurs every 2–7 years, with a cycle peak at 4 years. [7-8]. The Walker Circulation plays a significant role in the development of ENSO and IOD, as described above. Nevertheless, the airflow at the IWC varies from that at the PWC. Under typical circumstances, an easterly wind results in greater SST in the southeastern Indian Ocean compared to the western region. This easterly wind pushes the warm water pool in the western Indian Ocean to the east, exactly in southeastern region of Indonesia. Under these circumstances, the convection process occurs in the southeastern region of Indonesia, which undergoes a period of abundant rainfall known as the wet season. An SSTA Southeastern (Western) above (below) normal conditions results in an IOD that is negative (positive). Consequently, Indonesia experiences a surplus (reduction) in rainfall [4, 9]. Saji Hameed identified the original IOD around 1999 as an SSTA that influenced the rainfall in Indonesia. This condition is characterized by a trapped anomaly of zonal winds in the Indian Ocean's equator region [10]. Initially, researchers believed that IODs were a result of ENSOs, but subsequent studies have demonstrated that IODs can occur independently of ENSOs [11]. The peak of Indian Ocean Dipole (IOD) events typically occurs between September and November [6] and quickly subsides throughout the winter, leading to the phenomenon known as seasonal lock [12].

The reason of this study is updating the ENSO and IOD status from 1940 to 2023, enabling diverse using such as those in the fields of fishing, climatology, agriculture, and related field research to utilize the information effectively. Another thing that is of interest to this study is the ENSO-IOD activity over the past 84 years. The updating the ENSO and IOD status is important because of ENSO and IOD are more than just sea-atmospheric interactions. Moreover, these two have been known to be driven by climate globally and locally [8], so the existence of these phenomena is also very influential on Indonesia's climate, especially rainfall [4], [11], [13], [14]. At least six studies have demonstrated that the ENSO-IOD phenomena is responsible for the extreme rainfall conditions that occur in Indonesia [15--20]. Indonesia's location between the Pacific Rim and the Indian Ocean explains why ENSO and IOD have such a significant effect on its rainfall. For example, when El Niño (La Niña) occurs, Indonesia

will experience a lack of rainfall. If there is a positive IOD (negative IOD) in the Indian Ocean, the situation will worsen, leading to increasingly dry conditions (getting wetter). ENSO and IOD phenomena will naturally recur at some point; it is the concern of certain parties, especially the government, to anticipate the impact. Because ENSO and IOD are natural phenomena with the non-normal distribution of time-series data the uncertainty is huge. The Wavelet can be used to analysis this data [8].

This study's objective is to analyze the local signal of the signals of Niño3.4 Index and Dipole Mode Index (DMI), which indicate ENSO and IOD, respectively. This analysis uses Morlet's Wavelet [8], because it excels at the periodic localization of a single signal that other methods, like the Fourier transformation, cannot do. This study uses the Morlet's Wavelet because, in comparison to other wavelets, such as the Paul wavelet, which has superior resolution in time, it has comparatively good resolution in frequency [21]. Using Wavelet because this method is widely used in climatology [7]. In detail, a wavelet changes signals locally in the frequency and time domains [22]. This phase of localization demonstrates the activity of the signal. We can predict their effects more accurately by categorizing these ENSO and IOD events into specific periods. The Material and Method section offers additional information regarding wavelets.

Material and Method

This study uses SST data from ERA5 for 84 years (January 1940–December 2023). This is monthly data with a resolution of 0.25°. Similar studies have widely used the high-resolution data generated by ERA5 as material. [11], [23-24]. Additionally, we using the ERA5 data because the available the long-time covered data.

The region that determines the DMI and the Niño3.4 Index, as depicted in Figure 1, is the Indian Ocean and the Pacific Rim, which constitute this study area. The IOD phenomena are quantized based on SSTA in the West Tropical Indian Ocean (WTIO) and the South East Tropical Indian Ocean (SETIO) region of the Indian Ocean. The gap in SSTA between the WTIO and the SETIO is the determining factor for the Dipole Mode Index (DMI), as illustrated in Equation (1)

$$DMI = WTIO_{SSTA} - SETIO_{SSTA}. \quad (1)$$

After calculating the DMI using the difference between the SSTAs in the WTIO and SETIO zones, we can compute the Nio3.4 index using the SSTA in the Nino3.4 region as Equation (2)

$$SSTA_{ij} = SST_{ij} - \overline{SST}_{ij} \quad (2)$$

$$\overline{SST}_{ij} = \sum_{j=1}^{n} \frac{SST_{ij}}{n} \quad (3)$$

$SSTA_{ij}$ is the anomaly in the i month of the j year, SST_{ij} is the actual data of the i month of the j year, $\overline{SST}_{ij}$ is the climatology in the i year j.

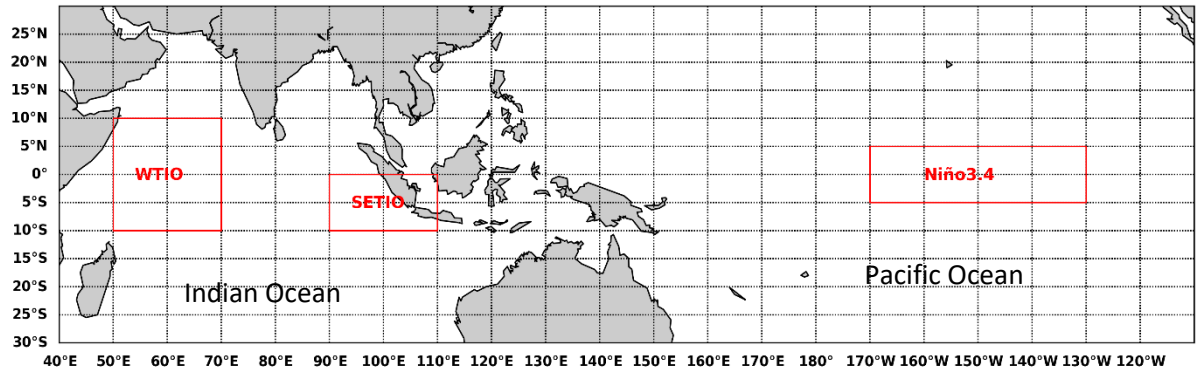

Figure 1. Research Area. The WTIO and SETIO are areas where SST anomalies occur, which show the DMI, while Niño3.4 is where SST anomalies occur, which show the Niño3.4.

This study classifies the DMI and the Niño3.4 index based on their standard deviation. However, the classification threshold for both indices is set at 0.5 [25]. The standard deviation, which serves as the upper and lower threshold for SSTA, is also employed by McKenna et al. [6]. Based on this criteria, McKenna et al. [6] find the IOD phenomena in seasonal. When the DMI and the Niño3.4 index are greater than positive (less than negative) standard deviations of each index, as indicated in Table 1, positive IODs and El Niño (negative IOD and La Niña) are defined.

Table 1. Niño3.4 index (X) and DMI (Y) classification.

No	X	Level	Y	Level
1	$X \geq 2$	Very Strong El Niño	$Y \geq 1.5$	Very Strong Positive IOD
2	$2 > X \geq 1.5$	Strong El Niño	$1.5 > Y \geq 1$	Strong Positive IOD
3	$1.5 > X \geq 1$	Moderate El Niño	$1 > Y \geq 0.5$	Moderate Positive IOD
4	$1 > X \geq Std$	Weak El Niño	$0.5 > Y \geq Std$	Weak Positive IOD
5	$-1 < X \leq -Std$	Weak La Niña	$-0.5 < Y \leq -Std$	Weak Negative IOD
6	$-1.5 < X \leq 1$	Moderate La Niña	$-1 < Y \leq 0.5$	Moderate Negative IOD
7	$-2 < X \leq 1.5$	Strong La Niña	$-1.5 < Y \leq 1$	Strong Negative IOD
8	$X \leq -2$	Very Strong La Niña	$Y \leq -1.5$	Very Strong Negative IOD

The previous section mentioned the use of Wavelet to obtain SSTA behavior over time, particularly the dominance of activity on a specific time scale. We conducted the analysis to examine the variance of the DMI and the Nio3.4 index over a period of 2 to 7 years. In the ENSO and IOD models [6], the most dominant time scale is 2-7 years/cycle, with the peak at 4 and 7 years/cycle. A wavelet is a function that transforms a signal into a new form. There are at least six types of wavelets [22], but this study uses only the Morlet form. This is because the Morlet form produces a better frequency-related localization of the period than any other form. The other wavelet, i.e., the Paul wavelet, has a better resolution in terms of time [21]. Basically, the Morlet wavelet is the result of a Gaussian function and exponential waves in their complex forms

$$\psi_0(\eta) = \pi^{-1/4} e^{i\omega_0 \eta} e^{-\eta^2/2}, \qquad (4)$$

with $\psi_0(\eta)$ adalah nilai is the value of a non-time-dependent wavelet η, and $\omega_0 = 6$ the initial frequency. To obtain local information about the signal, perform the transformation through the Continuous Wavelet Transform (CWT)

$$W_{n'}(s) = \sum_{n=0}^{N-1} x_n \, \psi^* \left[\frac{(n'-n)\delta t}{s}\right], \quad (5)$$

with ψ^* is the conjugate complex of ψ and n is expressing the time localization result on a particular scale s, while x_n is the time-series data to $n = 1,2,3 \cdots N$ with a time-space δt. In this case, x_n is the DMI and the Niño index3.4.

Result and Discussion

Figure 2 shows the relative standard deviations of the DMI and Niño3.4 index, which are 0.2 and 0.8. This suggests that the Sea Surface Temperature Anomaly (SSTA) in the Indian Ocean is lower in comparison to the SSTA in the Pacific Ocean. This statistical analysis shows that most of ENSO events align with the IOD. This result relates to Polonsky and Torbinsky's research [9] showing the relationship between ENSO and IOD. These phenomena have implications for Indonesia, particularly in conditions that get wetter (drier) during the wet (dry) season. Logically, this affects Indonesia's position between the Indian and Pacific oceans. Walker's circulation around the equator, which connects the Indian Ocean to the Pacific Ocean, demonstrates the indirect correlation between the DMI and the Niño3.4 index [6], [25].

Figure 2 and Table 1 depict the incidences of ENSO and IOD. According to the classification, it is observed that over the past 84 years, there have been 9 occurrences of El Niño (4) and La Niña, which align with positive IOD (negative IOD). Furthermore, El Niño and La Niña events occur approximately once and three times per year, respectively. El Niño and La Niña are caused by abnormal storm patterns in the northern Pacific Ocean, leading to fast variations in sea surface temperatures in the region. In addition, the analysis also shows that El Niño and La Niña are generally interannual phenomena [26], beginning in June-August of the first year and ending in March-May of the second year. However, the La Niña event that occurred from 1998 to 2000 had a duration of twelve months, making it the longest recorded period among all observed years. Ren, et at [27] also indicated that La Niña took place for 24 months. Generally, positive and negative IODs are a season-lock phenomenon, which means they only occur over a period of one year, starting in June-August and ending in September-October [11], [12]. However, SSTs in the western Pacific Ocean appear to be warmer (colder) at the start of the year, a phenomenon known as IOD-like positive (IOD-like negative). Both of these phenomena occur 3 (2) times each during the year of observation. The IOD-like positive (IOD-like negative) occur in 1993, 1994, and 1977(1985 and 2016), as shown in Table 2. Physically, this happens because of the fast-changing monsoon, especially in the Indian Ocean [12]. Some IOD-Like also shown by Shang-Min, et al [28] although different years of occurrence. These differences depend, of course, on the length of the observation data and the limits used. The DMI and the Niño Index3.4 also showed that in 1963, positive SSTAs in the Niño3.4 area did not meet the deviation standard, which meant they did not show that El Niño was happening, as Nur'utami, et al [25] and Ren, et at [27] said. Another interesting result is the ENSO-IOD anomaly phenomenon in 2002-03. During this period, El Nino occurred along with negative

IOD. This caused dry conditions in Indonesia to not last long or caused the western (eastern) region of Indonesia to experience a wet (dry) season.

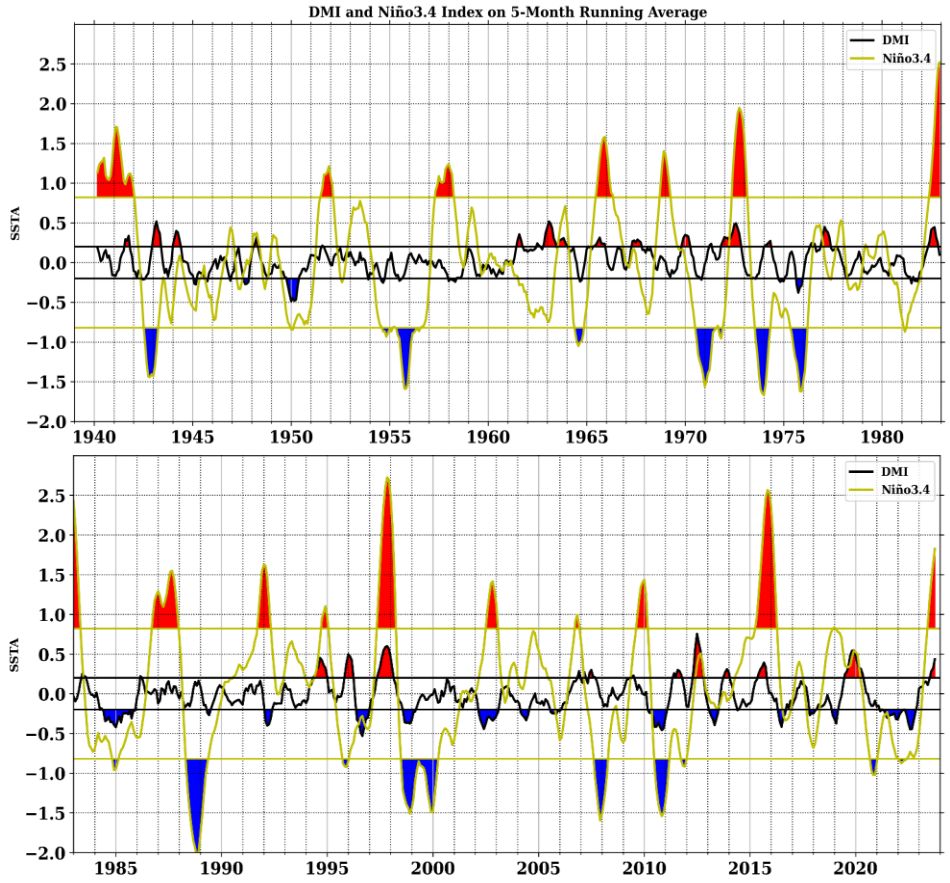

Figure 2. Five Months in the Running Average of SSTA for the DMI is represented by the black line, and the yellow line for the Niño3.4 Index. Standard deviations of the DMI and Niño3.4 Index are represented by vertical lines (yellow and black). The presence of a red fill represents the occurrence of El Niño and Positive IOD, whereas a blue fill shows the presence of La Niña and Negative IOD. In order to ensure that the SSTA occurs within a minimum of 5 months, we use a 5-month rolling average.

Table 2. The subscripts A and B show that El Niño and La Niña occur together with positive and negative IOD, respectively. The subscript L denotes the presence of positive and negative Indian Ocean Dipole (IOD)-like conditions, while Lc denotes the occurrence of El Nino and La Niña events between seasons. Subscript C represents the inverse occurrence. The symbols *, **, ***, and **** represent stages of weakness, moderation, strength, and very high strength, respectively.

El Niño	Positive IOD	La Niña	Negative IOD
1940/41$_{A}$***; 1952/53**; 1957/58**; 1965/66$_{A}$***; 1968/69$_{A}$**; 1972/73$_{A}$***; 1982/83$_{A}$****; 1986/87**; 1991/92***; 1994/95$_{A}$*; 1997/98$_{A}$****; 2002/03$_{C}$**; 2006 $_{Lc}$*; 2009/10**; 2015/16$_{A}$****;	1941$_{A}$*; 1943$_{L}$**; 1944$_{L}$*; 1961*; 1963*; 1965$_{A}$*; 1967*; 1969$_{A}$*; 1972$_{A}$*; 1977 $_{L}$*; 1982$_{A}$*; 1994$_{A}$*; 1995*; 1996$_{L}$*; 1997$_{A}$**; 2011*; 2012**; 2013*; 2015$_{A}$*; 2019**; 2023$_{A}$*	1942/43**; 1955/56***; 1964$_{Lc}$*; 1970/71**; 1972/73***; 1975/76$_{B}$***; 1984/85$_{B}$*; 1988/89****; 1995$_{Lc}$*; 1998-2000$_{B}$**; 2004$_{Lc}$*; 2007/08**; 2010/11$_{B}$**; 2013$_{Lc}$*;	1947*; 1949*; 1975$_{B}$*; 1984$_{B}$*; 1985$_{L}$*; 1992$_{L}$*; 1996**; 1998$_{B}$*; 2002$_{C}$*; 2010$_{B}$*; 2016$_{L}$*; 2021*; 2022*; 2018*; 2020*

Figure 3 shows the DMI power spectrum, which indicates the spread of DMI in the period's domain. Figure 3 (a) reveals that the inter-seasonal period saw DMI activity in 1993–2023 (0.5–1 years), while the 2-4-year period saw DMI activity in 1995–2000 and 2009–2019. It means that from 1993 to 2023 (1995 to 2000 and 2009 to 2019), the peak of DMI was in 0.5 – 1(2 - 4) year/cycle. It shows the DMI activity gains in the 1993 to 2023 period. However, some physical aspect for this event are not shown yet in this research. From 1940 to 1990, we observed DMI activity on a scale of more than 4 years. Although significant activity occurred during 1974–1983, this activity represents the peak of significant DMI, as shown in Figure 3. (b). Figure 3 (c) not only bases DMI activity on the power spectrum but also illustrates it through variance. Along with the power spectrum, the DMI variance also shows an increasing in the 2–7 year period scale. Based on this variance, we can identify at least three groups of variances based on the time scale: 1940–1968, 1969–1991, and 1992–2023.

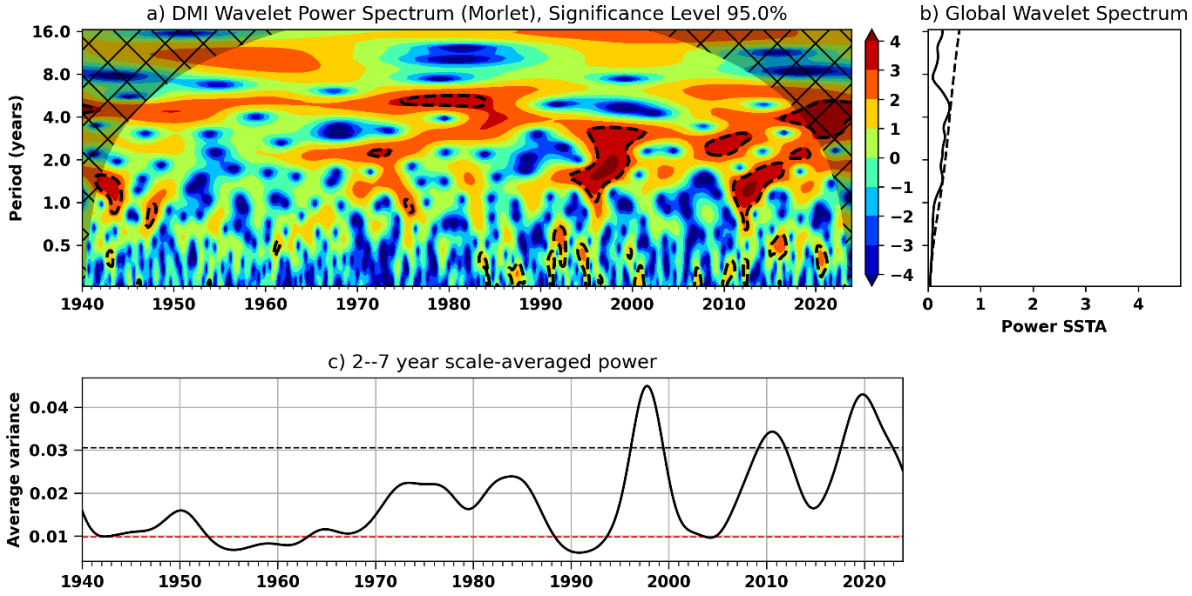

Figure 3. DMI Wavelet Power Spectrum (a), Magnitude (b), and 2-7 year scale average power (c). Dash black(red) line is significancy level at 95% (deviation standard). Color gradation indicates DMI activity.

Figure 4 displays the power spectrum of the Niño3.4 index. The power spectrum also describes the activity of Niño3.4 in various periods. Figure 4 (a) reveals that the dominant Niño3.4 activity takes place between 2 - 7 years. Sreedevi [29] also showed no significant differences in results. Significant positive activity occurred around 1970–2000. After 2000, Niño3.4 activity fell again until 2023. This shows that in the 1970–2000 period, the intensity (frequency) of ENSO was stronger (lower) than in the period after 2000. An increase in SST around the 20° region is the cause [30]. The variance in Figure 4 (c) aligns with the increase in Niño3.4 activity around 1970–2000. Fig. 4 (b) shows that this peak of Niño3.4 activity occurs over a period of more than 8 years, although this is not significant.

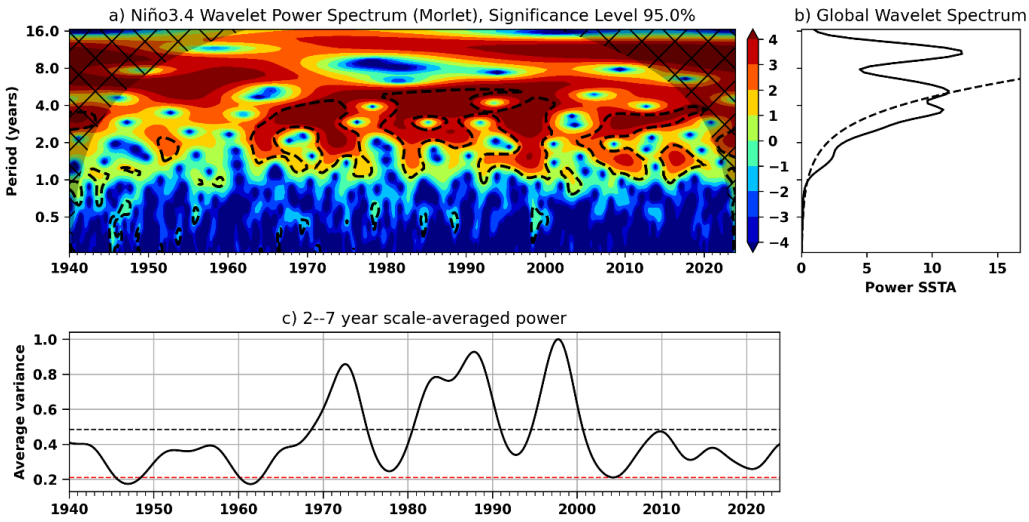

Figure 4. Same as **Figure 3**, but for Niño3.4 index.

Conclusion

Analysis of SSTA in the DMI and Niño3.4 region spanning 84 years reveals that certain occurrences of IOD are independent of the ENSO, as prior research has indicated. [11]. Furthermore, as is usually the case, ENSO happens concurrently with IOD, but El Niño happens in 2002–03 concurrently with negative IOD. The outcome deviated from the anticipated result. Additional research is required to gain a comprehensive understanding of the ENSO-IOD phenomenon, especially within the same calendar year. Apart from this unusual ENSO-IOD event, the analysis results also show five ENSO events that did not continue in the second year and several IODs that occurred at the beginning of the year. Subsequently, we determined that this IOD was indeed an occurrence resembling an IOD. Additionally, the Wavelet's analysis variance revealed that IOD activity was rising throughout the 1940–1968, 1969–1991, and 1992–2023 periods, whereas ENSO activity decreased once more during the 2000–2023 period following an increase during the 1970–2000 period [30]. The IOD variance also indicates that in the period 2000–2023, IOD was more dominant in climate conditions, especially rainfall in Indonesia. Based on Wang's analysis [30], which showed the causes of ENSO changes before and after 2000, we suspect the same thing was also the cause of increased IOD activity during the periods 1940–1968, 1969–1991, and 1992–2023. Nevertheless, this requires further investigation and proof.

Acknowledgment

We thankful to ECMWF in available the Sea Surface Temperature ERA5 data at https://cds.climate.copernicus.eu/cdsapp#!/dataset/reanalysis-era5-pressure-levels?tab=overview. We also thankful to editor and reviewer for improvement comments on for this article.

References

[1] X.-Y. Wang *et al.*, "Underestimated responses of Walker circulation to ENSO-related SST anomaly in atmospheric and coupled models," *Geosci. Lett.*, vol. 8, no. 1, p. 17, 2021, doi: 10.1186/s40562-021-00186-8.

[2] T. Bayr, D. Dommenget, and M. Latif, "Walker circulation controls ENSO atmospheric feedbacks in uncoupled and coupled climate model simulations," *Clim. Dyn.*, vol. 54, no. 5–6, pp. 2831–2846, 2020, doi: 10.1007/s00382-020-05152-2.

[3] H. Lopez, S. K. Lee, D. Kim, A. T. Wittenberg, and S. W. Yeh, "Projections of faster onset and slower decay of El Niño in the 21st century," *Nat. Commun.*, vol. 13, no. 1, pp. 1–13, 2022, doi: 10.1038/s41467-022-29519-7.

[4] D. Lestari, E. Sutriyono, S. Kadir, and I. Iskandar, "Respective Influences of Indian Ocean Dipole and El Niño - Southern Oscillation on Indonesian Precipitation," *J. Math. Fundam. Sci.*, vol. 50, pp. 257–272, 2018, doi: 10.5614/j.math.fund.sci.2018.50.3.3.

[5] D. Gushchina, I. Zheleznova, A. Osipov, and A. Olchev, "Effect of various types of ENSO events on moisture conditions in the humid and subhumid tropics," *Atmosphere (Basel).*, vol. 11, no. 12, 2020, doi: 10.3390/atmos11121354.

[6] S. McKenna, A. Santoso, A. Sen Gupta, A. S. Taschetto, and W. Cai, "Indian Ocean Dipole in CMIP5 and CMIP6: characteristics, biases, and links to ENSO," *Sci. Rep.*, vol. 10, no. 1, pp. 1–13, 2020, doi: 10.1038/s41598-020-68268-9.

[7] J. M. Polanco-Martínez, J. Fernández-Macho, and M. Medina-Elizalde, "Dynamic wavelet correlation analysis for multivariate climate time series," *Sci. Rep.*, vol. 10, no. 1, pp. 1–11, 2020, doi: 10.1038/s41598-020-77767-8.

[8] K. A. Tamaddun, A. Kalra, and S. Ahmad, "Wavelet analyses of western us streamflow with ENSO and PDO," *J. Water Clim. Chang.*, vol. 8, no. 1, pp. 26–39, 2017, doi: 10.2166/wcc.2016.162.

[9] A. Polonsky and A. Torbinsky, "The iod–enso interaction: The role of the Indian Ocean current's system," *Atmosphere (Basel).*, vol. 12, no. 12, 2021, doi: 10.3390/atmos12121662.

[10] Y. Xiao, Y. Tang, X. Tan, Y. Wu, and Z. Yao, "The SST–Wind Causal Relationship during the Development of the IOD in Observations and Model Simulations," *Remote Sens.*, vol. 14, no. 5, 2022, doi: 10.3390/rs14051064.

[11] A. Kurniadi, E. Weller, S. K. Min, and M. G. Seong, "Independent ENSO and IOD impacts on rainfall extremes over Indonesia," *Int. J. Climatol.*, vol. 41, no. 6, pp. 3640–3656, 2021, doi: 10.1002/joc.7040.

[12] S. Il An, H. J. Park, S. K. Kim, J. Shin, S. W. Yeh, and J. S. Kug, "Intensity changes of Indian Ocean dipole mode in a carbon dioxide removal scenario," *npj Clim. Atmos. Sci.*, vol. 5, no. 1, pp. 1–8, 2022, doi: 10.1038/s41612-022-00246-6.

[13] I. Iskandar *et al.*, "Evolution and impact of the 2016 negative Indian Ocean Dipole," *J. Phys. Conf. Ser.*, vol. 985, no. 1, 2018, doi: 10.1088/1742-6596/985/1/012017.

[14] Suhadi, I. Iskandar, Supari, M. Irfan, and H. Akhsan, "Extreme Drought Assessment in Sumatra-Indonesia Using SPI and EDI," *Sci. Technol. Indones.*, vol. 8, no. 4, pp. 691–700, 2023, doi: 10.26554/sti.2023.8.4.691-700.

[15] E. Hermawan *et al.*, "Characteristics of the Extreme Rainfall over Indonesian Equatorial Region based on the Madden-Julian Oscillation Index Data Analysis," *J. Phys. Conf. Ser.*, vol. 1373, no. 1, 2019, doi: 10.1088/1742-6596/1373/1/012002.

[16] D. Lestari, E. Sutriyono, Sabaruddin, and I. Iskandar, "Severe Drought Event in Indonesia Following 2015/16 El Niño /positive Indian Dipole Events," in *Journal of Physics: Conference Series*, 2018. doi: 10.1088/1742-6596/1011/1/012040.

[17] Supari, F. Tangang, L. Juneng, and E. Aldrian, "Observed changes in extreme

temperature and precipitation over Indonesia," *Int. J. Climatol.*, vol. 37, no. 4, pp. 1979–1997, 2017, doi: 10.1002/joc.4829.

[18] S. Supari, R. Muharsyah, and N. Wahyuni, "Impact of the 2015 Godzilla El Niño event on the Indonesian rainfall," *Sci. J. PPI - UKM*, vol. 3, no. 1, 2016, [Online]. Available: http://www.kemalapublisher.com/index.php/ppi-ukm/article/view/160

[19] Supari, F. Tangang, E. Salimun, E. Aldrian, A. Sopaheluwakan, and L. Juneng, "ENSO modulation of seasonal rainfall and extremes in Indonesia," *Clim Dyn*, vol. 51, no. 7–8, pp. 2559–2580, 2018, doi: 10.1007/s00382-017-4028-8.

[20] H. Akhsan, M. Irfan, Supari, and I. Iskandar, "Dynamics of Extreme Rainfall and Its Impact on Forest and Land Fires in the Eastern Coast of Sumatra," *Sci. Technol. Indones.*, vol. 8, no. 3, pp. 403–413, 2023, doi: 10.26554/sti.2023.8.3.403-413.

[21] M. Haddad, M. F. Belbachir, and S. Kahlouche, "Variability of El Niño-Southern oscillation from 1880 to 2010 revealed by wavelet analysis," *Int. J. Phys. Sci.*, vol. 6, no. 25, pp. 6036–6041, 2011, doi: 10.5897/IJPS10.618.

[22] S. Dyllon and P. Xiao, "Wavelet Transform for Educational Network Data Traffic Analysis," *Wavelet Theory Its Appl.*, 2018, doi: 10.5772/intechopen.76455.

[23] C. C. Crossett, A. K. Betts, L. A. L. Dupigny-Giroux, and A. Bomblies, "Evaluation of daily precipitation from the era5 global reanalysis against ghcn observations in the northeastern united states," *Climate*, vol. 8, no. 12, pp. 1–14, 2020, doi: 10.3390/cli8120148.

[24] Z. Ahmad Zul Amal, V. Mutya, and M. Marzuki, "Impact of different ENSO positions and Indian Ocean Dipole events on Indonesian rainfall." Vietnam Journal of Earth Sciences, pp. 100–119, 2024. doi: https://doi.org/10.15625/2615-9783/19926.

[25] M. N. Nur'utami and R. Hidayat, "Influences of IOD and ENSO to Indonesian Rainfall Variability: Role of Atmosphere-ocean Interaction in the Indo-pacific Sector," *Procedia Environ. Sci.*, vol. 33, pp. 196–203, 2016, doi: 10.1016/j.proenv.2016.03.070.

[26] A. Santoso, M. J. Mcphaden, and W. Cai, "The Defining Characteristics of ENSO Extremes and the Strong 2015/2016 El Niño," *Rev. Geophys.*, vol. 55, no. 4, pp. 1079–1129, 2017, doi: 10.1002/2017RG000560.

[27] H. L. Ren, B. Lu, J. Wan, B. Tian, and P. Zhang, "Identification Standard for ENSO Events and Its Application to Climate Monitoring and Prediction in China," *J. Meteorol. Res.*, vol. 32, no. 6, pp. 923–936, 2018, doi: 10.1007/s13351-018-8078-6.

[28] L. Shang-Min, L. Gen, H. Kaiming, and Y. Jun, "Origins of the IOD-like Biases in CMIP Multimodel Ensembles: The Atmospheric Component and Ocean–Atmosphere Coupling," *J. Clim.*, vol. 33, no. 24, pp. 10455–10467, 2020, doi: 10.1175/JCLI-D-20-0459.1.

[29] V. Sreedevi, S. Shamna, S. Adarsh, B. Amina, S. Surya, and P. Arun Krishna, "Multiscale Analysis of Drought Teleconnections of West Central India Using Wavelet Coherence," *Proc. 6th Int. Conf. Model. Simul. Civ. Eng.*, no. Icmsc 2022, pp. 129–136, 2023, doi: 10.21467/proceedings.156.18.

[30] R. WANG and H. L. REN, "The linkage between two ENSO types/modes and the interdecadal changes of ENSO around the year 2000," *Atmos. Ocean. Sci. Lett.*, vol. 10, no. 2, pp. 168–174, 2017, doi: 10.1080/16742834.2016.1258952.